Interlayer Magnetoresistance due to Chiral Soliton Lattice Formation in Hexagonal Chiral Magnet $CrNb_3S_6$

Y. Togawa,[1,2,*] Y. Kousaka,[3] S. Nishihara,[4] K. Inoue,[4,5] J. Akimitsu,[3] A. S. Ovchinnikov,[6] and J. Kishine[7]

[1]*N2RC, Osaka Prefecture University, 1-2 Gakuencho, Sakai, Osaka 599-8570, Japan*
[2]*JST, PRESTO, 4-1-8 Honcho Kawaguchi, Saitama 333-0012, Japan*
[3]*Department of Physics and Mathematics, Aoyama Gakuin University, Sagamihara, Kanagawa 252-5258, Japan*
[4]*Department of Chemistry, Faculty of Science, Hiroshima University, Higashi-Hiroshima, Hiroshima 739-8526, Japan*
[5]*IAMR, Facility of Science, Hiroshima University, Higashi-Hiroshima, Hiroshima 739-8530, Japan*
[6]*Institute of Natural Sciences, Ural Federal University, Ekaterinburg 620083, Russia*
[7]*Division of Natural and Environmental Sciences, The Open University of Japan, Chiba 261-8586, Japan*

(Received 29 August 2013; revised manuscript received 2 October 2013; published 7 November 2013)

We investigate the interlayer magnetoresistance (MR) along the chiral crystallographic axis in the hexagonal chiral magnet $CrNb_3S_6$. In a region below the incommensurate-commensurate phase transition between the chiral soliton lattice and the forced ferromagnetic state, a negative MR is obtained in a wide range of temperature, while a small positive MR is found very close to the Curie temperature. Normalized data of the negative MR almost falls into a single curve and is well fitted by a theoretical equation of the soliton density, meaning that the origin of the MR is ascribed to the magnetic scattering of conduction electrons by a nonlinear, periodic, and countable array of magnetic soliton kinks.

DOI: 10.1103/PhysRevLett.111.197204 PACS numbers: 75.25.−j, 72.15.Eb, 75.47.−m, 75.50.Cc

Materials with structural chirality, i.e., left or right handedness, are found at all length scales in nature from molecules to biological systems and bring in a wide variety of functionality [1]. In condensed matter physics, such materials can be found also among magnetic systems. Magnetic crystals such as $Fe_{1-x}Co_xSi$ [2], MnSi [3], and $Ba_2CuGe_2O_7$ [4], belong to chiral space groups and are frequently referred to as chiral magnets. In chiral magnets, the combined effect of the symmetric Heisenberg exchange and the antisymmetric Dzyaloshinskii-Moriya (DM) interactions caused by the relativistic spin-orbit interaction [5,6] gives rise to a nontrivial spin texture and various interesting functions unique to chiral magnets. A coupling of conduction electrons with nontrivial spin textures has recently attracted great attention because of the ability to manipulate magnetotransport properties such as the topological Hall effect [7]. One promising candidate to realize this coupling is the chiral soliton lattice (CSL), which is formed in a chiral magnet under magnetic fields perpendicular to the chiral axis. The CSL is a nonlinear array of magnetic soliton kinks. It is naturally expected that each magnetic soliton kink works as a strong scattering potential for itinerant spins. Therefore, decreasing the number of magnetic soliton kinks may reduce the magnetoresistance (MR) and thus the CSL will present a nontrivial MR.

In this Letter, we report the MR along the chiral axis in a hexagonal chiral magnetic crystal of $CrNb_3S_6$. We find that the normalized data of the negative MR almost falls into a single curve, and the revealed behavior indicates that the origin of the MR can be attributed to the magnetic scattering of conduction electrons by a nonlinear, periodic, and countable array of magnetic soliton kinks. Namely, we clarify the direct correlation between the experimentally measured MR and the analytically obtained soliton density as a function of the magnetic field.

$CrNb_3S_6$ is a typical monoaxial chiral magnet, which belongs to the space group of $P6_322$ [8]. It has a layered hexagonal structure of $2H$-type NbS_2 intercalated by Cr atoms, so often expressed as $Cr_{1/3}NbS_2$. The size of the unit cell is 0.57 nm in the ab plane and 1.21 nm along the c axis [9,10]. Cr atoms are in the trivalent state and have localized electrons with spins of $S = 3/2$, whereas conduction electrons are in an unfilled hybridized band of Nb and S. As a consequence of the chiral space group, the monoaxial DM interaction is allowed along the chiral c axis in $CrNb_3S_6$, which is given in the form of $-\boldsymbol{D} \cdot \boldsymbol{S}_1 \times \boldsymbol{S}_2$ between localized neighboring spins $\boldsymbol{S}_1$ and $\boldsymbol{S}_2$ at Cr atoms. Here, $\boldsymbol{D}$ represents the DM vector.

The DM interaction competes with Heisenberg ferromagnetic (FM) exchange coupling (J), resulting in the emergence of the chiral helimagnetic order (CHM) of spins along the c axis at zero magnetic field [5,6], as shown in Fig. 1(a). The period is given by $L(0) = 2\pi a_0/\arctan(D/J) \simeq 2\pi(J/D)a_0$ with a_0 being the atomic lattice constant along the chiral axis, which is incommensurate with respect to the underlying crystal. The sign of $\boldsymbol{D}$ determines the direction of spin rotation, namely, the chirality of the CHM. The period of the CHM is found to be about 48 nm, which gives $D/J \sim 0.16$ in $CrNb_3S_6$.

Under the magnetic field perpendicular to the chiral axis, the CHM transforms into a nonlinear magnetic superlattice of the CSL, as shown in Fig. 1(a). The CSL consists of forced FM regions periodically partitioned by chiral soliton

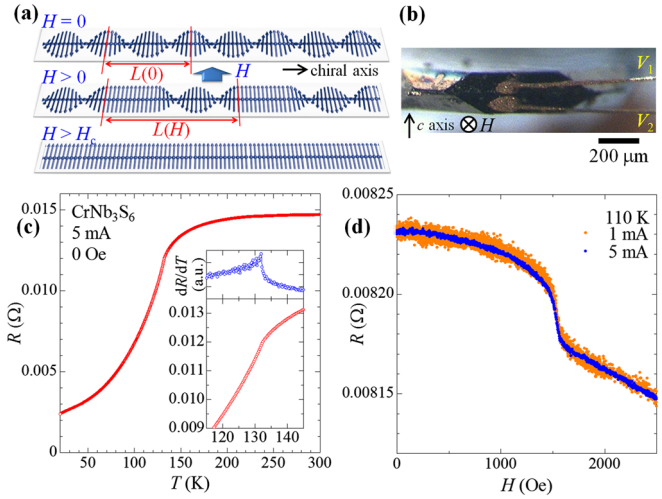

FIG. 1 (color online). (a) Schematic illustration of chiral magnetic orders. Spins of localized electrons rotate perpendicularly along the chiral axis because of the DM interaction, giving rise to the CHM at $H = 0$. In a magnetic field perpendicular to the chiral axis, the CHM continuously transforms into the CSL. Above H_c, the CSL turns into the forced FM state. (b) An optical micrograph of the ac plane of a $CrNb_3S_6$ single crystal with two electrodes for voltage detection. The other two electrodes for current application on the top and bottom surfaces (ab plane) are not visible. The magnetic field is applied in the direction perpendicular to the chiral c axis during the interlayer MR measurements. (c) Temperature dependence of the interlayer resistance at zero magnetic field. The insets show an enlarged view of the resistance close to T_C of 132 K and a temperature derivative of the resistance dR/dT. (d) The interlayer MR for a current of 1 and 5 mA at 110 K.

kinks of spins. The period of the CSL, $L(H)$, increases gradually with increasing magnetic field. Eventually, the CSL turns into the commensurate forced FM state above the critical magnetic field H_c [11–13].

The transformation process is regarded as the continuous incommensurate-commensurate (IC-C) phase transition from the CSL to the forced FM state, which is well described by the effective one-dimensional chiral sine-Gordon model [11–17]. Consequently, the CSL appears as the ground state unique to chiral magnetic crystals in the magnetic field.

The chiral sine-Gordon model is solved analytically. Importantly, the order parameter of the IC-C phase transition is provided by the soliton density $L(0)/L(H)$, which is theoretically given by $L(0)/L(H) = \pi^2/4K(\kappa)E(\kappa)$. Here, $K(\kappa)$ and $E(\kappa)$, respectively, denote the elliptic integrals of the first and second kinds with the elliptic modulus κ ($0 \leq \kappa \leq 1$) [18]. The critical field strength of the IC-C phase transition is expressed as $H_c = (\pi a_0 Q_0/4)^2 JS$. Then, the modulus κ is given by $\kappa/E(\kappa) = \sqrt{H/H_c}$. H_c corresponds to $\kappa = 1$. As a result, the soliton density $L(0)/L(H)$ monotonically decreases toward zero as a function of H/H_c.

Recently, the emergence and transformation of the CSL into the forced FM state have been experimentally verified in a thin $CrNb_3S_6$ single crystal by means of simultaneous real-space and k-space experiments using Lorentz transmission electron microscopy and the small-angle electron scattering method [19]. Applying a magnetic field perpendicular to the chiral c axis gives rise to the continuous growth of $L(H)$ from 48 nm toward infinity (sample size) at H_c, the behavior of which is well fitted by the soliton density $L(0)/L(H)$ based on the scenario of the CSL formation.

The CSL works as a tunable magnetic superlattice potential for itinerant spins. It is theoretically proposed that a novel type field-induced metal-to-insulator transition is caused by tuning the period of the CSL [17]. Thus, the magnetotransport properties will be interesting in the magnetic system where the CSL appears.

The in-plane (ab plane) resistance was investigated in a series of $3d$ transition metal intercalated dichalcogenides in the late 1970s [20,21], although the existence of the CSL had not been recognized yet in these materials at that time. Various physical properties including the in-plane MR were reported very recently in $CrNb_3S_6$ [22], although there is no report on the interlayer MR so far. Naively speaking, the interlayer MR along the chiral c axis would directly couple with the magnetic superlattice of the CSL and reflect the nature of the CSL rather than the in-plane MR.

$CrNb_3S_6$ single crystals are grown using the chemical vapor transport method. The crystals obtained frequently have a hexagonal platelet shape. Large and thick crystals with typical dimensions of a few millimeters diameter in the ab plane and a few hundred micrometers thickness along the c axis are chosen to examine the quality of the crystal by using x-ray diffraction, magnetization, and resistance measurements. Among them, only the crystals that show no indication of other phases are selected to measure the interlayer MR intensively. Representative data for a particular piece of a $CrNb_3S_6$ single crystal with a 1.5 mm diameter and 200 μm thickness are presented in the following.

The interlayer resistance data is taken by the standard four-terminal ac resistance measurement using a Quantum Design physical property measurement system. Each electrode, made by painting and postbaking a gold paste to obtain an ohmic contact with a low value of the contact resistance, is attached to a fine gold wire of 10 μm diameter. Two of the electrodes for voltage detection are located on the side surface (ac plane) of the hexagonal crystal with a separation of 5 μm at the closest gaps, as shown in Fig. 1(b), while the latter two for current application are put on the top and bottom surfaces (ab plane). The amplitude of the ac current ranges from 1 to 10 mA at a frequency of 137 Hz.

Figure 1(c) shows the temperature dependence of the interlayer resistance at zero magnetic field. The phase

transition temperature T_C is found to be 132 K, defined as the peak in the derivative of the resistance with respect to temperature dR/dT. Although the present value of T_C is slightly larger than typical values reported in the literature [19], it might reflect the very high quality of the crystal investigated.

The interlayer MR is measured with a step of 2 Oe in a range of the magnetic field up to 3 kOe. The magnetic field is altered so as to prevent it from overshooting a targeted value and kept constant in a superconducting persistent current mode. The magnetic field is applied perpendicular to the c axis while the electric current flows along the c axis. In this configuration, the magnitude of the anisotropic magnetoresistance should be the same irrespective of the spin configuration of the chiral magnetic orders formed in $CrNb_3S_6$ under magnetic fields perpendicular to the c axis since it predominantly orients within the ab plane and thus is always perpendicular to the current flow direction. Therefore, the contribution of the anisotropic magnetoresistance to the interlayer MR is considered as a constant background in our experiments.

Figure 1(d) shows the interlayer MR taken with a current of magnitude of 1 and 5 mA at 110 K. Both MR curves coincide with each other, indicating that no Joule heating occurs in this range of the current, although the data at 1 mA is rather noisy because of the small magnitude of the voltage signal and the lower measurement sensitivity to detect it. The interlayer MR exhibits a steep decrease toward 1570 Oe at 110 K. This value is quite consistent with H_c of the IC-C phase transition between the CSL and the forced FM state, which is determined by the magnetization measurement as explained later. Thus, the onset of the steep kink observed in the interlayer MR can be regarded as an indication of H_c. Above H_c, the interlayer MR decreases almost linearly with respect to the magnetic field. This behavior is in accord with that observed in the forced FM state in conventional FM materials. Indeed, such a tendency has been confirmed up to 20 kOe in the same specimen (not shown).

The interlayer MR is measured at 5 mA systematically as a function of temperature, as shown in Figs. 2(a) and 2(b). A negative change of the interlayer MR toward H_c is found in a wide range of temperature up to 125 K, as observed at 110 K in Fig. 1(d). The hysteresis behavior is not observed in the range of temperature investigated. The MR change becomes positive in a narrow region of the temperature between 125 K and T_C. The position of H_c indicated by a black arrow shifts toward lower magnetic fields with increasing temperature.

The MR ratio, defined as $(R_0 - R_c)/R_c$, is shown in Fig. 2(c). Here, R_0 and R_c correspond to the interlayer resistance at 0 Oe and H_c, respectively. The MR ratio takes a maximum of approximately 5.8% around 10 K and decreases gradually with increasing temperature. As described above, it becomes negative above 125 K. In this regime close to T_C, the formation of the CSL with dominating ferromagnetic

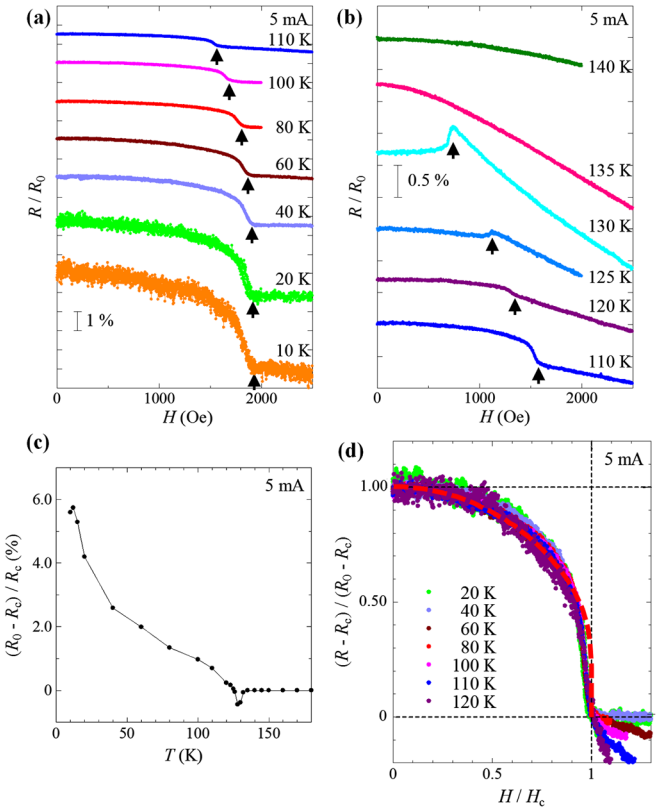

FIG. 2 (color online). The interlayer MR at 5 mA in a temperature range from 10 to 180 K. (a) A negative MR observed at low temperatures. (b) The MR changes positively above 125 K and decreases monotonically above T_C. Each MR curve is normalized by R_0 and given in arbitrary units in (a) and (b). The onset of the MR change indicated by a black arrow corresponds to H_c. (c) The MR ratio, defined as $(R_0 - R_c)/R_c$, is given as a function of temperature. (d) Normalized MR curves in a temperature region where a negative MR is observed. These curves are qualitatively fitted by a theoretical equation of the soliton density $L(0)/L(H)$ as indicated by a red broken line.

regions between kinks suppresses the magnetic scattering of the conduction electrons.

Figures 2(d) present a set of the normalized negative MR curves. They almost fall into a single curve and are qualitatively fitted by a theoretical equation of the soliton density $L(0)/L(H)$. This behavior means that the origin of the MR is ascribed to the magnetic scattering of the conduction electrons by a nonlinear, periodic, and countable array of the magnetic soliton kinks. Particularly, the MR curves show good coincidence with the soliton density change in a low magnetic field, where the total number of magnetic soliton kinks in CSL is as large as $\sim 4 \times 10^3$ in the present crystal with a dimension of 200 μm thickness. However, they deviate slightly close to H_c because the number of magnetic soliton kinks rapidly becomes very small in a high magnetic field and thus other factors will be more influential in causing the MR.

The empirical scaling law of the MR behavior indicates that the magnitude of the MR is in proportion to the

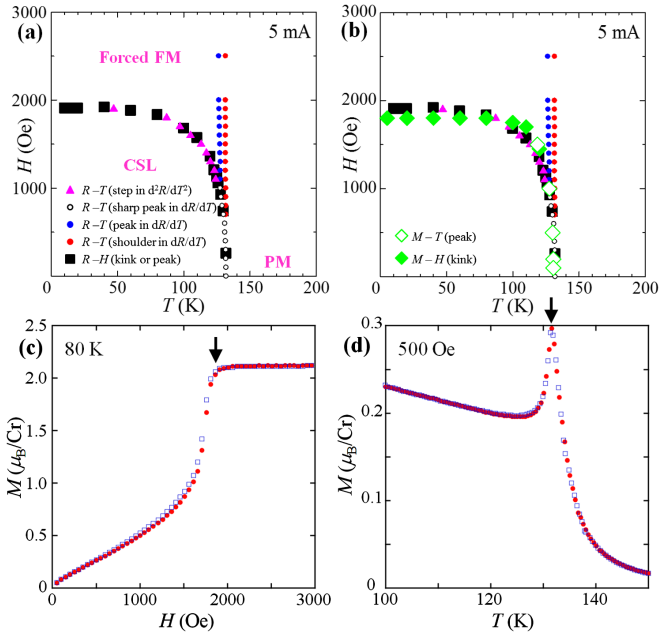

FIG. 3 (color online). The magnetic phase diagram of $CrNb_3S_6$. (a) Various kinds of anomalies found in the interlayer magnetotransport measurement as a function of magnetic field and temperature. (b) Comparison with the magnetization data. The magnetization data is shown as a function of magnetic field and temperature in (c) and (d), respectively. There is no hysteresis behavior of the data during the increasing (red solid circle) and decreasing (blue open square) processes. Black arrows indicate the position of kink and peak in the M-H and M-T measurements, respectively.

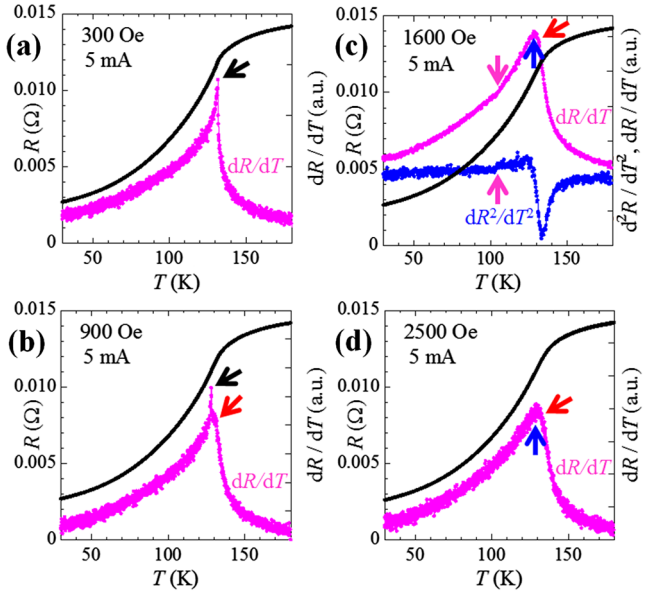

FIG. 4 (color online). Temperature dependence of the interlayer resistance with a current of 5 mA at various magnetic fields. (a) 300, (b) 900, (c) 1600, and (d) 2500 Oe. The sharp peak in dR/dT (magenta dots, labelled aside by letters) is indicated by a black arrow in (a) and (b), while the stepwise anomaly in d^2R/dT^2 (blue dots, labelled aside) is pointed out by a magenta arrow in (c). The shoulder structure (red oblique arrow) appears with a maximum (blue vertical arrow) at a lower magnetic field in dR/dT in (c) and (d).

number of magnetic soliton kinks. In other words, in the present specimen, the MR change due to the CSL formation is noticeable since the magnitude of the MR becomes giant with the piling up of the magnetic soliton kinks, although the resistance by a single magnetic soliton kink is a hundred times smaller than the total MR change.

The magnetic phase diagram is provided solely based on the interlayer MR data in Fig. 3(a). The solid square indicates the onset of the interlayer MR change, while other symbols correspond to the positions of anomalies found in the R-T measurements, as described in Fig. 4. It has been already reported in the literature that H_c of the IC-C phase transition between the CSL and the forced FM state can be identified by characteristic anomalies found in the magnetization data [13,23], as indicated in Figs. 3(c) and 3(d). Importantly, H_c values determined by two different ways are very consistent with each other, as shown in Fig. 3(b). Based on the experimental evidence that the interlayer MR traces quite well the continuous IC-C phase transition between the CSL and the forced FM state, it is concluded that the interlayer conduction process directly couples with the magnetic superlattice associated with the CSL formation and leads to the interlayer MR.

Since the CSL is a thermodynamic stable phase, it is natural to expect a signature even when sweeping temperature instead of magnetic field. Figure 4 shows the temperature dependence of the interlayer resistance at various magnetic fields. At a low magnetic field, a sharp peak is found in dR/dT in Fig. 4(a), as seen at zero magnetic field in Fig. 1(c). With an increase of the magnetic field, the sharp peak in dR/dT shifts slightly toward lower temperature, although the shoulder structure is left behind around the position corresponding to T_C.

As the magnetic field increases, furthermore, the sharp peak structure disappears in dR/dT. Instead, a stepwise change is found in d^2R/dT^2, as shown in Fig. 4(c). Its position clearly coincides with H_c determined by the interlayer MR measurements. At 2500 Oe, which is above H_c at low temperature, the interlayer resistance curve becomes featureless except that the shoulder structure appears with a maximum at a lower magnetic field in dR/dT. This structure remains even in higher magnetic fields above H_c and might be related to the spin fluctuation from the ordered forced FM state to the fluctuating paramagnetic state.

In conclusion, we have investigated the interlayer MR in the monoaxial chiral magnet $CrNb_3S_6$. It is found that the transformation from the CSL into the forced FM state gives rise to a negative MR toward H_c in a wide range of temperature below the IC-C phase transition. Our data indicate that the CSL works as a tunable magnetic superlattice potential for itinerant spins and the magnitude of the MR correlates well with the population of the magnetic

soliton kinks. Consequently, a giant MR is caused by a proliferation of magnetic soliton kinks. We stress that this mechanism can be realized in a single crystal of the monoaxial chiral magnet because of the robust coherence of the CSL. It is not so easy to realize the same situation in an array of magnetic domain walls in a ferromagnetic narrow stripe. The mechanism of the MR presented in this Letter, unique to the tunable and countable CSL protected by crystal chirality, may open up a route to a new paradigm for spin electronics applications using chiral magnetic crystals.

*y-togawa@21c.osakafu-u.ac.jp

[1] G. H. Wagniere, *On Chirality and the Universal Asymmetry* (Wiley-VCH, Weinheim, 2007).
[2] S. V. Grigoriev, V. A. Dyadkin, D. Menzel, J. Schoenes, Yu. O. Chetverikov, A. I. Okorokov, H. Eckerlebe, and S. V. Maleyev, Phys. Rev. B **76**, 224424 (2007).
[3] Y. Ishikawa, K. Tajima, D. Bloch, and M. Roth, Solid State Commun. **19**, 525 (1976).
[4] A. Zheludev, G. Shirane, Y. Sasago, N. Kiode, and K. Uchinokura, Phys. Rev. B **54**, 15163 (1996).
[5] I. E. Dzyaloshinskii, J. Phys. Chem. Solids **4**, 241 (1958).
[6] T. Moriya, Phys. Rev. **120**, 91 (1960).
[7] A. Neubauer, C. Pfleiderer, B. Binz, A. Rosch, R. Ritz, P. Niklowitz, and P. Böni, Phys. Rev. Lett. **102**, 186602 (2009).
[8] T. Moriya and T. Miyadai, Solid State Commun. **42**, 209 (1982).
[9] S. S. P. Parkin and R. H. Friend, Philos. Mag. B **41**, 65 (1980).
[10] T. Miyadai, K. Kikuchi, H. Kondo, S. Sakka, M. Arai, and Y. Ishikawa, J. Phys. Soc. Jpn. **52**, 1394 (1983).
[11] I. E. Dzyaloshinskii, Sov. Phys. JETP **19**, 960 (1964).
[12] Y. A. Izyumov, Sov. Phys. Usp. **27**, 845 (1984).
[13] J. Kishine, K. Inoue, and Y. Yoshida, Prog. Theor. Phys. Suppl. **159**, 82 (2005).
[14] I. G. Bostrem, J. Kishine, and A. S. Ovchinnikov, Phys. Rev. B **78**, 064425 (2008); A. B. Borisov, J. Kishine, I. G. Bostrem, and A. S. Ovchinnikov, Phys. Rev. B **79**, 134436 (2009).
[15] J. Kishine and A. S. Ovchinnikov, Phys. Rev. B **79**, 220405 (R) (2009).
[16] J. Kishine, A. S. Ovchinnikov, and I. V. Proskurin, Phys. Rev. B **82**, 064407 (2010).
[17] J. Kishine, I. V. Proskurin, and A. S. Ovchinnikov, Phys. Rev. Lett. **107**, 017205 (2011).
[18] M. Abramowitz and I. A. Stegun, *Handbook of Mathematical Functions* (Dover, New York, 1964).
[19] Y. Togawa, T. Koyama, K. Takayanagi, S. Mori, Y. Kousaka, J. Akimitsu, S. Nishihara, K. Inoue, A. S. Ovchinnikov, and J. Kishine, Phys. Rev. Lett. **108**, 107202 (2012).
[20] S. S. P. Parkin and R. H. Friend, Philos. Mag. B **41**, 95 (1980).
[21] S. S. P. Parkin and R. H. Friend, Physica (Amsterdam) **99B**, 219 (1980).
[22] N. J. Ghimire, M. A. McGuire, D. S. Parker, B. Sipos, S. Tang, J.-Q. Yan, B. C. Sales, and D. Mandrus, Phys. Rev. B **87**, 104403 (2013).
[23] Y. Kousaka, Y. Nakao, J. Kishine, M. Akita, K. Inoue, and J. Akimitsu, Nucl. Instrum. Methods Phys. Res., Sect. A **600**, 250 (2009).